Type III secretion system effector proteins are mechanically labile

Marc-André LeBlanc[a,b], Morgan R. Fink[a], Thomas T. Perkins[b,c,1], and Marcelo C. Sousa[a,1]

[a]Department of Biochemistry, University of Colorado, Boulder, CO 80309; [b]JILA, National Institute of Standards and Technology and University of Colorado, Boulder, CO 80309; and [c]Department of Molecular, Cellular, and Developmental Biology, University of Colorado, Boulder, CO 80309

Edited by Jorge E. Galán, Yale University, New Haven, CT, and approved February 16, 2021 (received for review September 16, 2020)

Multiple gram-negative bacteria encode type III secretion systems (T3SS) that allow them to inject effector proteins directly into host cells to facilitate colonization. To be secreted, effector proteins must be at least partially unfolded to pass through the narrow needle-like channel (diameter <2 nm) of the T3SS. Fusion of effector proteins to tightly packed proteins—such as GFP, ubiquitin, or dihydrofolate reductase (DHFR)—impairs secretion and results in obstruction of the T3SS. Prior observation that unfolding can become rate-limiting for secretion has led to the model that T3SS effector proteins have low thermodynamic stability, facilitating their secretion. Here, we first show that the unfolding free energy (ΔG^0_{unfold}) of two *Salmonella* effector proteins, SptP and SopE2, are 6.9 and 6.0 kcal/mol, respectively, typical for globular proteins and similar to published ΔG^0_{unfold} for GFP, ubiquitin, and DHFR. Next, we mechanically unfolded individual SptP and SopE2 molecules by atomic force microscopy (AFM)-based force spectroscopy. SptP and SopE2 unfolded at low force ($F_{unfold} \leq 17$ pN at 100 nm/s), making them among the most mechanically labile proteins studied to date by AFM. Moreover, their mechanical compliance is large, as measured by the distance to the transition state ($\Delta x^\ddagger = 1.6$ and 1.5 nm for SptP and SopE2, respectively). In contrast, prior measurements of GFP, ubiquitin, and DHFR show them to be mechanically robust ($F_{unfold} > 80$ pN) and brittle ($\Delta x^\ddagger < 0.4$ nm). These results suggest that effector protein unfolding by T3SS is a mechanical process and that mechanical lability facilitates efficient effector protein secretion.

type III secretion system | single-molecule force spectroscopy | atomic force microscopy | unfolding free energy | protein stability

Type III secretion systems (T3SS) are large nanomachines utilized by both pathogenic and symbiotic bacteria to inject effector proteins directly into the cytoplasm of host cells (1–3). Once delivered, effector proteins facilitate host cell colonization through a variety of mechanisms (4–7), including down-regulation of the host immune response (8) and rearrangement of the cytoskeleton (9, 10). The T3SS apparatus, known as the injectisome, is a syringe-like structure with a hollow needle that spans the inner and outer bacterial membranes, the extracellular space, and the host membrane, enabling proteins to pass directly from bacteria to host cells (Fig. 1*A*) (2). Specialized bacterial chaperones often bind the N-terminal 50 to 100 amino acids (aa) of the effector proteins, known as the chaperone binding domain, and help maintain the effector N-terminal domain in an extended conformation. C-terminal to the chaperone binding domain, effector proteins contain one or more globular domains, which adopt their folded conformations even when in complex with their cognate chaperone (4, 11, 12). The effector proteins, or their chaperone complexes, are recognized by the base of the injectisome prior to secretion (13). At its narrowest point, the injectisome needle's inner diameter is less than 2 nm (14–16). As a result, effector proteins must be mostly unfolded to be secreted (17–20). Secretion is thus thought to proceed by a "threading-the-needle mechanism," where the N-terminal extended domain is released from the chaperone and fed to the injectisome, followed by unfolding of the C-terminal effector domain (21).

Before proteins are secreted through the T3SS, they interact with a hexameric ATPase at the base of the T3SS that is capable of mediating chaperone release from effector proteins and effector-protein unfolding (15, 22). Indeed, most in vivo unfolding is catalyzed by unfoldases that work from one end of the substrate protein in stark contrast to the global effects of temperature, pH, or chemical denaturants. The most common examples of targeted protein unfolding are catalyzed by ATPases of the AAA(+) family that mechanically unfold their substrates (23, 24). For example, the AAA(+) ATPase ClpX forms a ring-shaped hexamer that mechanically pulls its substrates through its narrow central pore to unfold them (25). These are powerful unfoldases that can unfold even tightly packed proteins such as GFP, ubiquitin, and dihydrofolate reductase (DHFR) (23, 24, 26, 27). However, the T3SS ATPase does not belong to the AAA(+) family of ATPases. Instead, it is structurally similar to the catalytic β-subunit of the F_1F_0 ATP synthase, a rotary motor that normally couples proton gradient dissipation to ATP synthesis but can also run in reverse and hydrolyze ATP to do work (15, 28–30). The T3SS ATPase is not as powerful an unfoldase as the AAA(+) family, as fusions of effector proteins with GFP, ubiquitin, or DHFR stall in the injectisome and are poorly secreted (20, 22, 31, 32). These observations have led to the current model that T3SS effector proteins have low thermodynamic stability to facilitate their secretion (22, 31–33).

While thermodynamic stability is the most common metric of protein stability, mechanical stability is a distinct metric that quantifies how easily a protein unfolds under force (F_{unfold}). Mechanical

Significance

The type III secretion system (T3SS) is an important virulence factor that enables some bacteria to directly inject effector proteins into host cells, facilitating colonization. To be secreted, effector proteins must be unfolded, and tightly packed proteins like GFP cannot be secreted through the T3SS, leading to the model that effector proteins have low thermodynamic stability. We show that two model effector proteins have thermodynamic stabilities similar to tightly packed proteins (GFP and ubiquitin) but are much more mechanically labile. These results strongly suggest that mechanical stability predicts whether a protein is compatible with secretion through the T3SS and may shed light on the distinct evolutionary pressures that resulted in the sequence divergence of effector proteins from their nonsecreted homologues.

Author contributions: M.-A.L., M.R.F., T.T.P., and M.C.S. designed research; M.-A.L. and M.R.F. performed research; M.-A.L., M.R.F., T.T.P., and M.C.S. analyzed data; and M.-A.L., M.R.F., T.T.P., and M.C.S. wrote the paper.

The authors declare no competing interest.

This article is a PNAS Direct Submission.

Published under the PNAS license.

[1]To whom correspondence may be addressed. Email: tperkins@jila.colorado.edu or Marcelo.Sousa@colorado.edu.

This article contains supporting information online at https://www.pnas.org/lookup/suppl/doi:10.1073/pnas.2019566118/-/DCSupplemental.

Published March 15, 2021.

Downloaded at CU Libraries on March 15, 2021

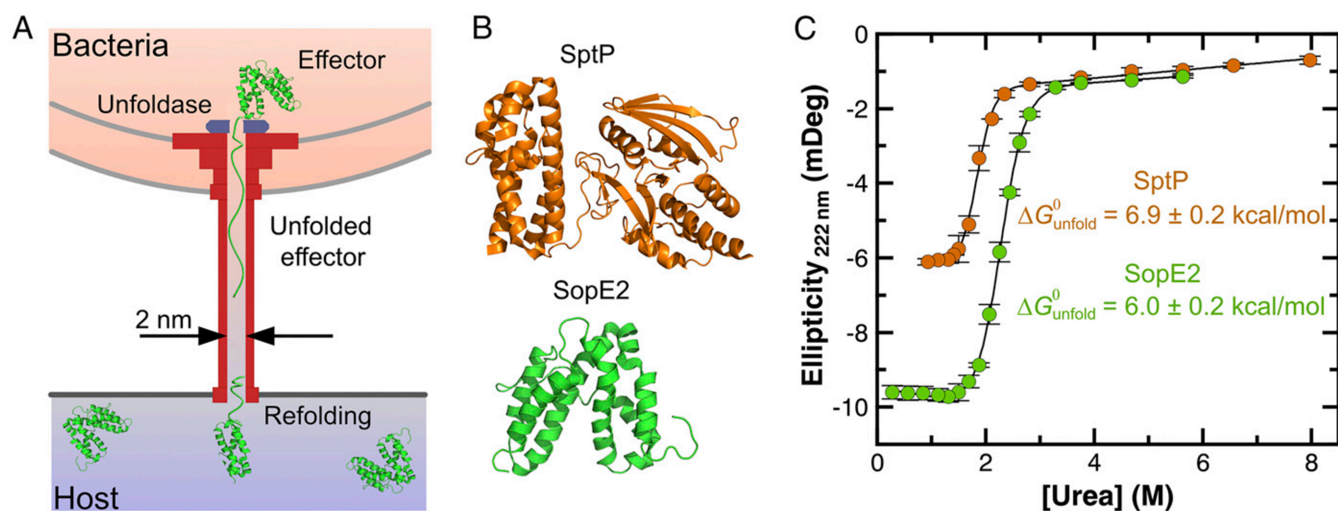

Fig. 1. Thermodynamic stability of T3SS effector proteins $SptP_{CD}$ and $SopE2_{CD}$. (*A*) Schematic depiction of protein transport through the T3SS showing effector proteins, which are at least partially folded in the bacterial cytoplasm. Such effector proteins interact with an associated unfoldase to passage through the T3SS, which has an inner channel with a diameter <2 nm. Once inside the host cytoplasm, effector proteins refold to carry out their function. (*B*) Crystal structures of $SptP_{CD}$ (Protein Data Bank [PDB] ID code 1G4U) and $SopE2_{CD}$ (PDB ID code 1R9K). (*C*) Ellipticity from CD at λ = 222 nm plotted as a function of urea concentrations for $SptP_{CD}$ (orange) and $SopE2_{CD}$ (green). A fit of the data with Eq. **1** yielded the free energy of unfolding ΔG^0_{unfold} for $SptP_{CD}$ (6.9 ± 0.2 kcal/mol [mean ± fit error]) and $SopE2_{CD}$ (6.0 ± 0.2 kcal/mol [mean ± fit error]). Data points are the result of at least three independent measurements. Error bars represent SD.

stability is typically measured by pulling across the N and C termini of single molecules via force spectroscopy using optical tweezers (34, 35) or an atomic force microscope (AFM) (36). Early force spectroscopy studies showed that thermodynamic stability does not correlate with mechanical stability (37–41). For example, titin's I28 domain requires ∼20% more force to unfold than titin's I27 domain [I85 and I91, respectively, in the new nomenclature (42)], despite I27 having approximately twofold higher thermodynamic stability (43). Importantly, AFM studies have shown that GFP (44), ubiquitin (45), and DHFR (46) are mechanically robust, requiring high forces to unfold despite their typical thermodynamic stabilities. These three proteins each stall the T3SS; thus, mechanical stability may be the physical determinant to proteins being secreted by the T3SS, rather than thermodynamic stability.

Here, we determine the thermodynamic and mechanical stabilities of SptP and SopE2, two effector proteins from *Salmonella enterica*. These effectors are ideal candidates for this study as they have known crystal structures (10, 47), have characterized in vivo secretion kinetics (48), and represent effector proteins of different size and structure (Fig. 1*B*). We show that the catalytic domains of SptP and SopE2 have unremarkable thermodynamic stabilities, similar to many other previously characterized proteins, including GFP, ubiquitin, and DHFR. Conversely, our AFM-based force spectroscopy measurements demonstrate that SptP and SopE2 are among the most mechanically labile proteins studied to date by AFM. These two T3SS effector proteins are therefore mechanically labile while being thermodynamically stable, supporting the hypothesis that it is mechanical stability, not thermodynamic stability, that predicts efficient protein secretion by the T3SS.

Results

Thermodynamic Stability of SptP and SopE2 Catalytic Domains. For effector proteins to be secreted through the narrow T3SS needle, they must first be unfolded. However, the injectisome cannot unfold tightly packed proteins such as GFP, ubiquitin, or DHFR, which block secretion (20, 22, 31, 32). The current model suggests that effector proteins have low thermodynamic stabilities to facilitate their unfolding and subsequent secretion. To test this model, we focused on *Salmonella enterica* SptP and SopE2. These well-characterized effectors consist of N-terminal chaperone binding domains, generally thought to be unstructured (17, 49), followed by well-folded catalytic domains whose crystal structures have been determined (10, 47) (Fig. 1*B*). To characterize their unfolding energetics, we expressed the folded catalytic domains of SptP ($SptP_{CD}$, residues 161 to 543) and SopE2 ($SopE2_{CD}$, residues 69 to 240) and measured their thermodynamic stability by collecting far-ultraviolet (UV) circular dichroism (CD) spectra at various concentrations of urea (Fig. 1*C*).

Far-UV CD spectra of purified $SptP_{CD}$ and $SopE2_{CD}$ recorded at 25 °C were consistent with well-folded proteins. Next, we screened for conditions to achieve reversible urea-induced unfolding of the proteins so that thermodynamic parameters could be extracted. As shown in *SI Appendix*, Fig. S1, $SptP_{CD}$ was reversibly unfolded by urea in 10 mM Tris, pH 8.0, 150 mM sodium sulfate, and 0.5 mM TCEP, while $SopE2_{CD}$ was reversibly unfolded by urea in 25 mM Hepes, pH 7.2, 150 mM NaCl, and 0.5 mM TCEP.

Under reversible unfolding conditions, we measured the ellipticity at λ = 222 nm of $SptP_{CD}$ and $SopE2_{CD}$ as a function of urea concentration (Fig. 1*C*). To extract the standard change in free energy of unfolding (ΔG^0_{unfold}), the data were fit to a two-state model and linearly extrapolated to zero denaturant concentration, as described by Clarke and Fersht (50). For $SptP_{CD}$, ΔG^0_{unfold} = 6.9 ± 0.2 kcal/mol (mean ± fit error), m = 3.7 $kcal \cdot mol^{-1} \cdot M^{-1}$ and C_m = 1.9 M, where m is the dependence of ΔG^0_{unfold} on denaturant concentration, and C_m is the concentration of denaturant at the equilibrium unfolding midpoint (see Eq. **1** in *Materials and Methods* for more details). For $SopE2_{CD}$, ΔG^0_{unfold} was 6.0 ± 0.2 kcal/mol (mean ± fit error) with m = 2.6 $kcal \cdot mol^{-1} \cdot M^{-1}$ and C_m = 2.3 M. These values of ΔG^0_{unfold} are typical for globular proteins [ΔG^0_{unfold} = 7.0 ± 2.9 kcal/mol (mean ± SD) for a representative set of 23 proteins compiled by Robertson and Murphy (51)]. Therefore, $SptP_{CD}$ and $SopE2_{CD}$ are not characterized by low thermodynamic stability.

High-Precision Single-Molecule Assay Shows SptP and SopE2 Are Mechanically Labile. Given the typical thermodynamic stabilities of $SptP_{CD}$ and $SopE2_{CD}$, we next investigated their mechanical

Downloaded at CU Libraries on March 15, 2021

stability to test if a protein's mechanical properties might correlate with their propensity to be secreted through the T3SS. We measured the mechanical stability of $SptP_{CD}$ and $SopE2_{CD}$ by unfolding individual molecules using AFM-based single-molecule force spectroscopy. Preliminary experiments demonstrated that both $SptP_{CD}$ and $SopE2_{CD}$ unfolded at low force. We therefore adopted an assay developed to measure the unfolding of mechanically labile proteins (52). We enhanced the assay by implementing a polyprotein with genetically encoded labels (53) to facilitate attachment and integrating focused-ion-beam-modified cantilevers for greater precision and temporal resolution (54, 55). The polyprotein (Fig. 2*A*) is composed of 1) an N-terminal ybbR tag (56) for covalent attachment to a coenzyme A (CoA)-derivatized, polyethylene glycol (PEG)-functionalized glass coverslip, 2) a well-characterized "marker" domain—the fourth domain of the F-actin cross-linking filamin rod of *Dictostelium discoideum* (ddFLN4)—which has a distinctive two-step unfolding pattern (57) that facilitates screening for single-molecule attachment, 3) the protein of interest ($SptP_{CD}$ or $SopE2_{CD}$), and 4) a dockerin domain for strong but reversible attachment to a cohesin-coated, PEG-functionalized AFM tip, yielding approximately threefold higher rupture force than streptavidin–biotin (53). The resulting assay thus featured site-specific, covalent conjugation of the polyprotein to a PEG-coated glass coverslip and a strong, but reversible, site-specific attachment to a PEG-coated cantilever (Fig. 2*A*).

The assay was initiated by gently pressing the cohesin-functionalized cantilever into the surface for a brief period (0.1 s) and then retracting the cantilever at a fixed velocity (v). Importantly, the PEG coating suppressed nonspecific adhesion between the tip and the surface that often obscures low-force unfolding events. In ~10% of the retractions, the resulting force-extension curves were consistent with stretching a single molecule, for both the $SptP_{CD}$ and $SopE2_{CD}$ polyprotein construct (Fig. 2 *B* and *C*). The rapid force drops correspond to the unfolding of individual protein domains, followed by an increase in tension as the unfolded polypeptide segment was further stretched by cantilever retraction. We color-coded the force-extension curves by the next domain to unfold, so the pair of rapid force drops in gray corresponds to the unfolding of ddFLN4 and the orange and green segments correspond to the initial unfolding of $SptP_{CD}$ and $SopE2_{CD}$ (Fig. 2 *B* and *C*, respectively). For both $SptP_{CD}$ and $SopE2_{CD}$, their initial unfolding at low extension were well resolved and the traces showed minimal tip-surface adhesion (Fig. 2 *B* and *C*, *Inset*).

To verify the assignment of this first force drop at low extension to the initial unfolding of $SptP_{CD}$ and $SopE2_{CD}$, we analyzed individual segments of the force-extension curves by fitting them to a worm-like chain model (36) (Fig. 2 *B* and *C*, dashed lines). Each such segment corresponds to pulling on an unstructured polypeptide of a fixed number of aa, allowing us to determine the change in contour length (ΔL_0) between unfolding peaks (58). ΔL_0 should match the expected difference in length between the known three-dimensional structure and the unfolded polypeptide, based on the number of aa unfolded and the distance between aa [0.36 nm/aa (59)]. This analysis yielded 129 ± 1 nm (mean ± SEM; n = 178) and 57.8 ± 0.4 nm (n = 234) for $SptP_{CD}$ and $SopE2_{CD}$, respectively, in good agreement with the expected values of 133 and 57.4 nm, respectively. Both $SptP_{CD}$ and $SopE2_{CD}$ unfolded at low force (16.5 ± 1.8 pN [mean ± SEM; n = 31 at 100 nm/s] and 12.6 ± 0.7 pN [n = 25]) despite their differences in size and structure (10, 47, 60, 61).

Quantifying the Mechanical Stability and Compliance of SptP and SopE2. To characterize the mechanical properties of $SptP_{CD}$ and $SopE2_{CD}$, we measured their initial unfolding forces over a broad range of retraction velocities, yielding their dynamic force spectra. To do so, the cantilever was retracted at five different pulling velocities (100 to 3,200 nm/s). The mean unfolding force for each protein was computed from a minimum of 20 traces at each velocity and showed a linear relation when plotted as a function of the logarithm of the loading rate ($\partial F/\partial t$), in agreement with the Bell–Evans model (62) (Fig. 2*D*). Fitting each dynamic force spectrum to the Bell–Evans model yielded the distance to the transition state ($\Delta x^{\ddagger}$), a measure of mechanical compliance characterizing how much a protein deforms along the stretching axis before unfolding, and the unfolding rate at zero force (k_0) (*SI Appendix*, Table S1). For $SptP_{CD}$ and $SopE2_{CD}$, the resulting mechanical compliance ($\Delta x^{\ddagger}$) was 1.5 ± 0.4 nm (mean ± fitting error) and 1.4 ± 0.2 nm, respectively. In contrast, $\Delta x^{\ddagger}$ for many proteins characterized by force spectroscopy range from 0.3 to 0.6 nm, as compiled by Hoffman et al. (60). Thus, SptP and SopE2 are among the most mechanically compliant proteins characterized to date by AFM.

Discussion

Implications for Type III Secretion. Most T3SS effector proteins, including SptP and SopE2, contain an N-terminal region that encodes a secretion signal followed by a chaperone binding domain.

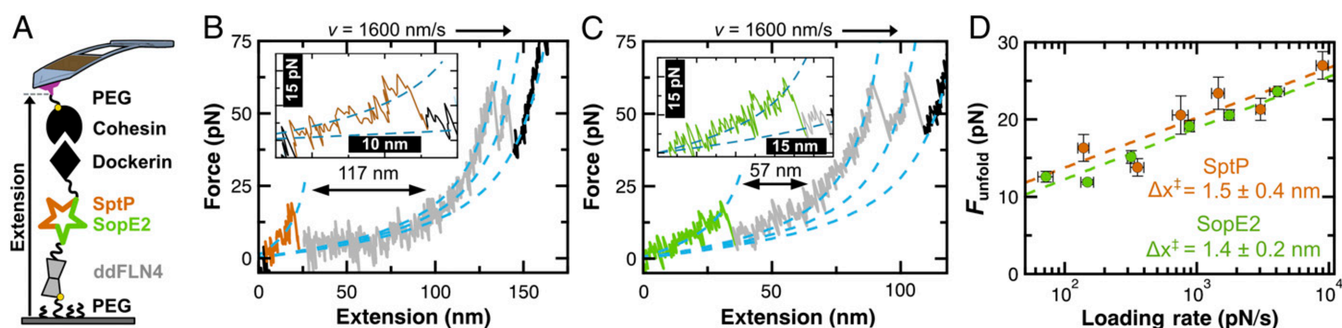

Fig. 2. Mechanical stability of T3SS effector proteins. (*A*) Schematic of AFM-based force spectroscopy assay shows the polyprotein construct site-specifically coupled to a PEG-functionalized glass coverslip. The polyprotein consisted of the protein of interest ($SptP_{CD}$ [orange] or $SopE2_{CD}$ [green]) positioned between a well-characterized marker protein ddFLN4 (gray) and dockerin (black). Cohesin (black) was site-specifically anchored to a PEG-functionalized AFM cantilever. The cohesin–dockerin interaction is mechanically very strong (F_{unfold} >300 pN at 600 nm/s) and thus dissociates after all the other proteins have unfolded. Extension is defined as the distance between the surface and the cantilever tip. (*B* and *C*) Representative force-extension curves at a constant pulling velocity (1,600 nm/s) show the unfolding of $SptP_{CD}$ (orange) and $SopE2_{CD}$ (green) as denoted by a sharp reduction in force followed by the characteristic double peaked unfolding of ddFLN4 (gray). Segments of the curve were well described by a worm-like chain model (dashed lines) and correspond to stretching a fixed amount of unstructured polypeptide. Data smoothed to 5 kHz. (*D*) Mean unfolding force (F_{unfold}) plotted as a function of loading rate for $SptP_{CD}$ (orange) and $SopE2_{CD}$ (green). Data points represent the averages of at least 20 individual unfolding events. Error bars represent the SEM. Analysis of this data with a Bell–Evans model (dashed lines) yielded the distance to the transition state ($\Delta x^{\ddagger}$) and the zero-force unfolding rate (k_0).

https://doi.org/10.1073/pnas.2019566118

Downloaded at CU Libraries on March 15, 2021

Together, these features are responsible for secretion targeting, and deletion of the chaperone binding domain results in loss of T3SS secretion for both proteins (63). These N-terminal domains adopt extended, largely unstructured conformations that wrap around the chaperone as observed for SptP in complex with its chaperone SicP (49) as well as several other effector/chaperone complexes (11, 64, 65). Effector functions are carried out by globular domains that are C-terminal to the chaperone binding domains. Secretion is thought to start by threading of the unstructured N termini through the base of the injectisome. This provides a primer for mechanical pulling of the effector globular domain through the injectisome, inducing its unfolding and secretion. However, tightly packed proteins, such as GFP, ubiquitin, and DHFR, cannot be easily unfolded by the T3SS and, fused to the C-termini of effectors, they impair or block their secretion (20, 22, 28, 31). This indicates that protein unfolding can be the rate-limiting step in secretion through the T3SS.

The current model used to explain these results proposes that effector proteins are less thermodynamically stable than the proteins that inhibit secretion. Consistent with this model, previous studies with the effector protein AvrPto showed a $\Delta G^0_{\mathrm{unfold}}$ as low as 1.0 kcal/mol at pH 6.1 (66). However, AvrPto is a short (164 aa) protein that belongs to a relatively small group of T3SS effectors, primarily restricted to the plant pathogen *Pseudomonas syringae*, whose secretion is chaperone-independent. As such, ArvPto does not have an N-terminal unstructured chaperone binding domain to prime mechanical unfolding. It is therefore possible that these small effectors are thermodynamically unstable such that a large fraction of protein is already unfolded ready for secretion without the need to be actively unfolded. Conversely, the globular domains of effector proteins that have unstructured chaperon binding domains, such as SptP and SopE2, were found to have higher, more typical thermodynamic stabilities. Studies of YopH and the catalytic domain of YopE found thermodynamic stabilities of 6 to 7 kcal/mol (11, 67), suggesting that the effector would need to be actively unfolded for efficient secretion.

Our measurements show that $\mathrm{SptP_{CD}}$ and $\mathrm{SopE2_{CD}}$ have thermodynamic stabilities of 6.9 ± 0.2 kcal/mol (mean ± fit error) and 6.0 ± 0.2 kcal/mol, respectively. These values are similar to the thermodynamic stabilities for GFP, ubiquitin, and DHFR found in the literature ($\Delta G^0_{\mathrm{unfold}}$ = 7.3, 6.0, and 5.9 kcal/mol, respectively) (68–70), which are proteins that cannot be efficiently secreted. When comparing $\Delta G^0_{\mathrm{unfold}}$ for these effector proteins to a broader set of proteins compiled by Robertson and Murphy (51), we observe that thermodynamic stabilities of $\mathrm{SptP_{CD}}$ and $\mathrm{SopE2_{CD}}$ are quite typical (Fig. 3*A*) (see Table 1 for a full list of proteins). Also notable, there is little correlation between secondary structure content or fold topology and thermodynamic stability (Fig. 3*A*). Hence, thermodynamic stability does not explain why effector proteins can be unfolded and secreted by the T3SS while GFP, ubiquitin, and DHFR cannot.

In contrast to their typical thermodynamic stabilities, $\mathrm{SptP_{CD}}$ and $\mathrm{SopE2_{CD}}$ both unfolded at low force (20.6 ± 2.5 pN [mean ± SEM] and 14.0 ± 0.5 pN, respectively, when pulling at 400 nm/s) and thus are mechanically labile. They also have large distances to the transition state $\Delta x^{\ddagger}$ (1.5 ± 0.4 nm [mean ± fit error] and 1.4 ± 0.2 nm, respectively) and thus are mechanically compliant. This is in stark contrast to the mechanical properties of the proteins that cannot be unfolded by the T3SS. Previous studies have shown that GFP, ubiquitin, and DHFR require much higher forces to unfold (116, 227, and 82 pN, respectively, when pulling at 600 nm/s) and they are "brittle," with short distances to the transition state $\Delta x^{\ddagger}$ (0.28, 0.23, and 0.37 nm, respectively) (44–46). The zero-force unfolding rates for $\mathrm{SptP_{CD}}$ and $\mathrm{SopE2_{CD}}$ are 0.2 ± 0.4 $\mathrm{s^{-1}}$ (value ± fitting error) and 0.7 ± 0.4, respectively. The extrapolated rate for GFP is a comparable 0.33 $\mathrm{s^{-1}}$ (71),

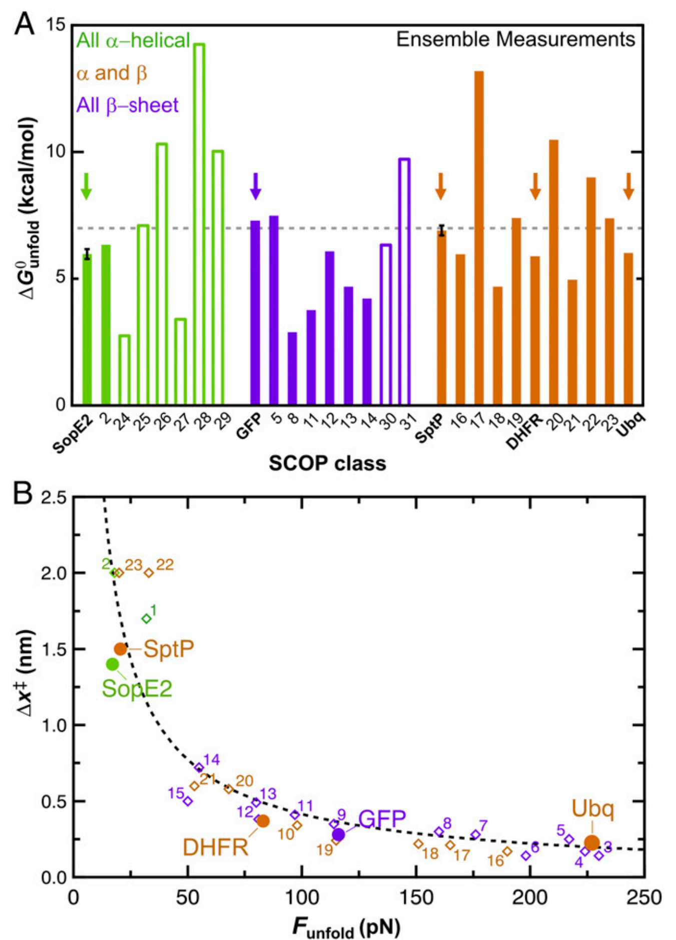

Fig. 3. Comparing thermodynamic and mechanical properties of $\mathrm{SptP_{CD}}$ and $\mathrm{SopE2_{CD}}$ with previously characterized reference proteins. (*A*) Ensemble thermodynamic stability ($\Delta G^0_{\mathrm{unfold}}$) for a series of proteins. Arrows indicate $\mathrm{SptP_{CD}}$ and $\mathrm{SopE2_{CD}}$ and three proteins that inhibit secretion through the T3SS (GFP, ubiquitin, and DHFR). Reference proteins were labeled with numbers (Table 1) and mostly cataloged in refs. 51 and 60. Colors correspond to the secondary structure of the protein, either all α-helical (green), α-helical and β-sheet (orange), or all β-sheet (purple) as defined by their structural classification of proteins (SCOP) class. Unfilled bars represent proteins for which $\Delta x^{\ddagger}$ and F_{unfold} has not been measured and therefore are not plotted in *B*. Dashed line indicates the average of all values ($\Delta G^0_{\mathrm{unfold}}$= 7.0 kcal/mol). Note that $\Delta G^0_{\mathrm{unfold}}$ for both $\mathrm{SptP_{CD}}$ and $\mathrm{SopE2_{CD}}$ is within 15% of this average. (*B*) The distance to the transition state ($\Delta x^{\ddagger}$) plotted as a function of mean unfolding force at v = 600 nm/s. Protein numbering and coloring is the same as in *A* (Table 1). The three proteins known to inhibit T3SS secretion are highlighted. The dashed line is a guide to the eye and represents the Bell–Evans model (62) for the most probable unfolding force $F_{\mathrm{unfold}} = (\Delta x^{\ddagger}/k_B T)^{-1}\ln[r\Delta x^{\ddagger}/(k_0 k_B T)]$ using a fixed loading rate (r = 200 pN/s) and zero force unfolding rate (k_0 = 0.2 $\mathrm{s^{-1}}$), that captures the overall trend for the mechanical properties of diverse proteins rather than the specifics of any individual protein.

while the rate extrapolated for ubiquitin is much longer (0.015 $\mathrm{s^{-1}}$) (72) despite both GFP's and ubiquitin's being incompatible with unfolding by the T3SS unfoldase. Thus, the values of zero-force unfolding rates as estimated by force spectroscopy did not correlate with secretion efficiency. Hence, in contrast to their thermodynamic stabilities and zero-force unfolding rates, the mechanical compliance and mechanical lability of GFP, ubiquitin, DHFR, $\mathrm{SptP_{CD}}$, and $\mathrm{SopE2_{CD}}$ correlate with their ability to be unfolded and secreted by the T3SS.

The unusually low unfolding forces and large distances to the transition state displayed by $\mathrm{SptP_{CD}}$ and $\mathrm{SopE2_{CD}}$ are highlighted

Downloaded at CU Libraries on March 15, 2021

Table 1. Thermodynamic and mechanical stability of $SptP_{CD}$ and $SopE2_{CD}$ compared with reference proteins called out in Fig. 3

No.	Protein name	PDB ID code	$\Delta x^{\ddagger}$, nm	F_{unfold} at 600* nm/s, pN	ΔG^{0}_{unfold}, kcal/mol	SCOP class	References
	$SptP_{CD}$	1G4U	1.5	20.5	6.9	α + β	
	$SopE2_{CD}$	1R9K	1.4	17	6.0	All α	
	Ubiquitin	1UBQ	0.23	227	6.0	α + β	45, 69
	GFP	1GFL	0.28	116	7.3	All β	44, 68
	DHFR:methotrexate†	1RG7	0.37	82	5.9	α + β	46, 70
1	Spectrin	1AJ3	1.7	32	N/A	All α	39
2	Cam DomC	1CFC	2	18	6.35	All α	82, 83
3	Fe-pfRD	1BRF	0.14	230	N/A	All β	84
4	1FNIII	1OWW	0.17	224	N/A	All β	38
5	I27	1TIT	0.25	217	7.5	All β	85
6	Zn-pfRD	1ZRP	0.14	198	N/A	All β	84
7	I27mut	1TIT	0.28	176	N/A	All β	60
8	Tn 3FNIII	1TEN	0.3	160	2.9	All β	86, 87
9	I1	1G1C	0.35	114	N/A	All β	38, 88
10	13FNIII	1FNH	0.34	98	N/A	All β	38
11	C2B	1TJX	0.41	97	3.8	All β	89, 90
12	10FNIII	1FNF	0.38	81	6.1	All β	38, 91
13	TmCspB	1G6P	0.49	80	4.7	All β	60, 92
14	C2A	2R83	0.72	55	4.2	All β	89, 90
15	ddFLN4	1KSR	0.5	50	N/A	All β	93, 94
16	Protein G	1PGA	0.17	190	6.0	α + β	95, 96
17	Top7	1QYS	0.21	165	13.2	α + β	97, 98
18	Protein L	1HZ6	0.22	151	4.7	α + β	99, 100
19	AVF3-109	2J6B	0.24	115	7.4	α + β	101
20	Barnase	1BNR	0.58	68	10.5	α + β	102, 103
21	AcP	ZAPS	0.6	53	5.0	α + β	104, 105
22	PAS-B	1X00	2	33	9.0	α + β	106, 107
23	RNase H	1RNH	2	20	7.4	α + β	35, 108
24	ACP apo	1ACP	N/A	N/A	2.8	All α	109
25	GCN4	2ZTA	N/A	N/A	7.1	All α	110
26	cyt *c*	1HRC	N/A	N/A	10.3	All α	111
27	Lac repressor	1LCD	N/A	N/A	3.4	All α	112
28	Myoglobin	4MBN	N/A	N/A	14.3	All α	113
29	Trp repressor	2WRP	N/A	N/A	10.0	All α	114
30	Plasminogen K4	1PMK	N/A	N/A	6.3	All β	115
31	Tendamistat	3AIT	N/A	N/A	9.7	All β	116

$\Delta x^{\ddagger}$ and F_{unfold} at 600 nm/s (pN) values are primarily sourced from Hoffman et al. (60). N/A, not assessed.

*Extrapolation to unfolding force at 600 nm/s where necessary.

†DHFR in vivo is likely bound to folate, so a ligand-bound result for DHFR is used to best capture its mechanical behavior in vivo.

when compared to an array of previously characterized proteins (Fig. 3*B*). Furthermore, the similarity in mechanical properties between $SptP_{CD}$ and $SopE2_{CD}$ is noteworthy, as $SopE2_{CD}$ is entirely α-helical while $SptP_{CD}$ contains β-sheets (Fig. 1*B*). In general, protein structures of mixed α/β content have exhibited lower compliance ($\Delta x^{\ddagger}$) and higher unfolding forces than proteins with all α-helical structures (Fig. 3*B*, orange vs. green), while proteins fully composed of β-sheets are the most mechanically robust and unfold at the highest forces (60) (Fig. 3*B*, purple).

A mechanistic consequence of effector proteins unfolding at very low force is that it allows weak unfoldases, such as those associated with the T3SS (22), to unfold them. This low-force unfolding primarily arises due to the large mechanical compliance of the effector proteins. We discuss this result within the context of the Bell model (73) where the rate of unfolding k under force is given by $k(F) = k_0 \exp(F\Delta x^{\ddagger}/k_B T)$, where $k_B T$ is the thermal energy. Therefore, $k(F)$ is linearly dependent on k_0 but exponentially dependent on $\Delta x^{\ddagger}$. Thus, at any given force exerted by an unfoldase, compliant proteins (large $\Delta x^{\ddagger}$) unfold more rapidly than brittle proteins (short $\Delta x^{\ddagger}$) given a fixed k_0 because the height of the transition state ($\Delta G^{\ddagger}$) for unfolding under force is lowered by $F\Delta x^{\ddagger}$, as illustrated in *SI Appendix*, Fig. S2.

The exponential dependence of k on $\Delta x^{\ddagger}$ underlies the hyperbolic-like shape of $\Delta x^{\ddagger}$ vs. F_{unfold} shown in Fig. 3*B*, a dependence previously noted (60). Stated differently, a large mechanical compliance facilitates protein unfolding because it allows unfoldases to accelerate unfolding by applying force gradually over larger distances (74). Interestingly, despite the vast diversity of proteins in Fig. 3*B*, we can capture the shape of the $\Delta x^{\ddagger}$-vs.-F_{unfold} plot using the Bell–Evans equation $F_{mp} = (\Delta x^{\ddagger}/k_B T)^{-1} \ln[r\Delta x^{\ddagger}/(k_0 k_B T)]$ (62) with r = 200 pN/s and k_0 = 0.2 s^{-1}, where F_{mp} is the most probable unfolding force and r is the loading rate (Fig. 3*B*, dashed line). (Note that these values of r and k_0 are typical for force spectroscopy of globular proteins. The exact values of r and k_0 are arbitrary as only the ratio of r/k_0 is constrained by the fit shown in Fig. 3*B*.) This observation highlights the role of $\Delta x^{\ddagger}$ in governing mechanical stability of this diverse array of proteins independent of any individual protein's k_0, its structural class (i.e., all α-helical or α/β mixture), and the exact loading rate.

When taken together, the low unfolding force and large distance to the transition state suggest that effector proteins have evolved specific structural elements that do not interfere with

BIOPHYSICS AND COMPUTATIONAL BIOLOGY

Downloaded at CU Libraries on March 15, 2021

their thermodynamic stability but make them highly amenable to mechanical unfolding. Interestingly, the aa sequences of effector proteins are notoriously divergent from those of nonsecreted homologs with similar structures (4, 75). We propose that the unique evolutionary pressure to select for mechanical lability to facilitate unfolding—while maintaining thermodynamic stability to ensure efficient refolding in the host—underlies the sequence divergence observed in T3SS effectors. Future studies can test this hypothesis by comparing the mechanical properties of T3SS effectors to structural homologs that are not secreted. Further future work can investigate applying force only locally by pulling one end of a molecule through a nanopore (76), as opposed to pulling across the N and C termini, as is standard for the force-spectroscopy field. The nanopore assay is technologically much more challenging when applying a calibrated force but it better mimics an unfoldase applying force to one end of an effector. Indeed, the local structure that the unfoldase encounters first can impact unfolding rates, as has been studied in bulk assays of the AAA+ ATPase/protease complex ClpXP using circularly permutated GFP as a substrate (27). More recently, this was also addressed in single-molecule studies of ClpA and ClpX, taking advantage of the fact that these AAA+ ATPases can be isolated as assembled hexamers with a central pore through which the substrate is pulled for unfolding (25, 77, 78).

In conclusion, our results strongly suggest that mechanical stability can predict whether a protein is compatible with secretion through the T3SS. Secretion kinetics and mechanical characterization of additional T3SS effector proteins are required to determine if mechanical stability is always rate-limiting for their secretion. SopE2 is secreted approximately twofold faster than SptP in vivo (48). However, their mechanical stabilities (both the unfolding force and their compliance) are similar. This suggests that once a protein is mechanically labile enough to pass through the T3SS other factors predominate in determining its secretion kinetics. Such factors could be as simple as the size of the protein (SptP is approximately twofold larger than SopE2) or may involve the complex interplay of chaperones with the T3SS sorting complex.

Materials and Methods

Protein Expression and Purification. All proteins were overexpressed in *Escherichia coli* BL-21 (DE3) cells transformed with the appropriate plasmid. The following protocol was used for the AFM polyproteins; details on the expression and purification of protein for CD experiments can be found in the *SI Appendix*. Cells were grown in 1-L cultures of Luria broth supplemented with kanamycin (50 μg/mL) and lactose auto-induction mixture (0.6% vol/vol glycerol, 0.05% wt/vol glucose, and 0.2% wt/vol lactose) (79) overnight at 37 °C. Cells were harvested and lysed with an Emulsiflex C3 homogenizer and protein was purified using Ni-NTA beads (Qiagen). The eluted protein was further purified using a Superdex 75 prep-grade column equilibrated with AFM measurement buffer (25 mM Hepes, pH 7.2, 150 mM NaCl, and 2 mM TCEP). Protein was aliquoted and snap-frozen with liquid nitrogen and stored at −80 °C.

CD Measurement and Analysis. Measurements were performed using a quartz cuvette (Hellma) with a 1-mm path length on an Applied PhotoPhysics ChiraScan Plus spectrophotometer. Measurement parameters were as follows: $\lambda = 212.5$ to 260 nm, step size = 0.5 nm, bandwidth = 1.0 nm, time per point = 0.5 s, and three repeats. The instrument was thoroughly purged with nitrogen to prevent ozone formation. Temperature was held at 25 °C with a Peltier sample holder and the temperature recorded using the temperature probe. Prior to loading, samples were spun at 18,000 rcf for 5 min. We measured a control sample as "blank" before every protein sample. Following this pair of measurements, the cuvette was serially rinsed with several milliliters each of 10 M urea, urea-free buffer, 1% cleaning solution (Hellmanex), and ultrapure water. The cuvette was then filled with ultrapure water and a CD spectrum taken to ensure no protein adhered to the cuvette. The cuvette was then rinsed with absolute ethanol and dried using filtered house air. This was repeated for every concentration of urea.

We analyzed the CD data using Applied Photophysics software. First, the three independent measurements were averaged. The subsequent spectrum was smoothed using the Savitzky–Golay algorithm with a window size of 12 points. This smoothing was done on both the protein-containing sample and the blank. We then subtracted the smoothed blank spectrum from the smoothed protein-containing spectrum to give the final, baseline corrected spectrum. After this analysis was done for all urea concentrations, the ellipicity at $\lambda = 222$ nm was plotted as a function of urea concentration. We then fit this plot with Eq. **1** to determine the free energy of unfolding assuming a two-state system which accounts for sloping baselines (50):

$$Y = \frac{(\alpha_{\text{fold}} + \beta[D]) + (\alpha_{\text{fold}} + \beta_{\text{unfold}}[D])\exp\left[\left(m[D] - \Delta G^0_{\text{unfold}}\right)/k_B T\right]}{1 + \exp\left[\left(m[D] - \Delta G^0_{\text{unfold}}\right)/k_B T\right]}, \quad [1]$$

where Y is the ellipticity; $[D]$ is the concentration of urea; α_{fold} and β_{fold} are the intercept and slope, which quantifies the sloping baseline of the folded state; α_{unfold} and β_{unfold} are the intercept and slope, which quantifies the sloping baseline of the unfolded state; m is the dependence of the free energy on the denaturant concentration; and $k_B T$ is thermal energy. The fit was weighted by the SD of each point where the data at each concentration are an average of measurements from three to five independent experiments.

Functionalization of AFM Cantilevers and Surfaces. Focused-ion-beam modified cantilevers with improved performance were made from commercial cantilevers (BioLever Mini; Olympus) using established protocols (54, 80). Maleimide-functionalized AFM cantilevers and glass coverslips were prepared as described previously (52). Briefly, focused-ion-beam (FIB)-modified cantilevers and KOH-cleaned glass coverslips were UV–ozone-irradiated for 30 min prior to incubation with silane-PEG-maleimide reagent (PG2-MLSL-600; Nanocs, Inc.) (0.15 mg/mL in toluene) for 3 h. After rinsing, cantilevers and surfaces were immediately reacted with CoA (1 mM in 50 mM sodium phosphate, pH 7.2, 50 mM NaCl, and 10 mM ethylenediaminetetraacetic acid) for 1 h at room temperature. After rinsing with ultrapure water, covalent protein coupling was carried out via the ybbR-tag to the CoA by the enzyme Sfp phosphopantetheinyl transferase (SFP) (56). To do so, aliquots of the cohesin and the polyprotein, stored at −80 °C (1 to 2 mg/mL), were individually thawed and diluted to 0.1 to 0.5 μM in Hepes buffer (25 mM Hepes, pH 7.2, and 150 mM NaCl) before adding $MgCl_2$ and SFP to final concentrations of 10 mM and 3 μM, respectively. These two protein mixtures were applied to the CoA-functionalized cantilevers (cohesin, 30 μL) or coverslips (polyprotein, 90 μL) and reacted for 1 h at room temperature. Cantilevers and coverslips were rinsed in Hepes buffer, loaded into the AFM, and allowed to settle for at least 30 min before measuring.

AFM Assay and Analysis. AFM experiments were performed on a Cypher ES (Asylum Research) in a temperature-controlled closed fluidic cell ($T = 25$ °C). The stiffness (k) of the FIB-modified cantilevers was calibrated using the thermal method (81) far from the surface, while sensitivity was measured by pressing the cantilever into hard contact with the surface. The cantilevers had an average $k \approx 6.5$ pN/nm. Force-extension curve acquisition was initiated by pressing the cantilever into the surface at 100 pN for 0 to 200 ms depending on the surface polyprotein concentration. This comparatively low indentation force was enabled by our site-specific, cohesin-dockerin-based coupling between the tip and the polyprotein. To minimize the compliance of the polyprotein construct, we used only a single marker domain and short PEG linkers (molecular weight = 600 Da), which facilitated detecting proteins that unfold at low force and low extension (Fig. 2 *B* and *C*, *Inset*). We retracted the cantilever at 100 to 3,200 nm/s while digitizing at 50 kHz. We acquired multiple traces per sample by probing the surface in a raster scan, moving the AFM tip in a grid pattern with each location separated by 150 nm. Each spot was probed 10 times unless a molecule was detected, in which case the spot was continually sampled until ~20 consecutive attempts failed to yield a connection. This meant that an individual protein could be repeatedly probed. We found that both $SopE2_{CD}$ and $SptP_{CD}$ refolded well, and repeated cycles of unfolding and refolding did not affect the observed unfolding forces (*SI Appendix*, Fig. S3). The high-bandwidth records were boxcar-averaged to the indicated bandwidths for analysis and presentation (1 to 5 kHz). Force was determined by cantilever deflection accounting for the sensitivity and stiffness of each cantilever. Extension was calculated from the movement of the sample stage minus the deflection of the cantilever. The loading rate (picoNewtons per second) for each unfolding event in a force-extension curve was calculated by fitting a line to the force-vs.-time curve immediately preceding effector protein unfolding. For the effector protein unfolding-force analysis, only the first unfolding event was used when an unfolding intermediate was observed. A small percentage of the

Downloaded at CU Libraries on March 15, 2021

force-extension curves showed atypically high unfolding forces for the initial unfolding of $SptP_{CD}$ $SopE2_{CD}$ (8 and 2%, respectively). These records were excluded from analysis as they most likely represented rare tip-sample surface adhesion and/or unfolding of a misfolded protein.

Data Availability. The data presented in this paper, including supplementary figures, are available via Dryad (https://datadryad.org/stash/dataset/doi:10.5061/dryad.0rxwdbrzv).

ACKNOWLEDGMENTS. We thank Devin Edwards for preparation of FIB-modified cantilevers, David Jacobson for discussions, and Prof. Hermann Gaub and his laboratory for providing DNA for elements of the polyprotein construct. This work was supported by NIH/CU Molecular Biophysics Graduate Traineeship T32 GM065103, the NSF (MCB-1716033), and National Institute of Standards and Technology (NIST). Mention of commercial products is for information only; it does not imply NIST's recommendation or endorsement. T.T.P. is a staff member of NIST's Quantum Physics Division.

1. J. E. Galán, M. Lara-Tejero, T. C. Marlovits, S. Wagner, Bacterial type III secretion systems: Specialized nanomachines for protein delivery into target cells. *Annu. Rev. Microbiol.* **68**, 415–438 (2014).
2. W. Deng *et al*., Assembly, structure, function and regulation of type III secretion systems. *Nat. Rev. Microbiol.* **15**, 323–337 (2017).
3. S. Wagner *et al*., Bacterial type III secretion systems: A complex device for the delivery of bacterial effector proteins into eukaryotic host cells. *FEMS Microbiol. Lett.* **365**, fny201 (2018).
4. J. E. Galán, Common themes in the design and function of bacterial effectors. *Cell Host Microbe* **5**, 571–579 (2009).
5. J. Diao, Y. Zhang, J. M. Huibregtse, D. Zhou, J. Chen, Crystal structure of SopA, a Salmonella effector protein mimicking a eukaryotic ubiquitin ligase. *Nat. Struct. Mol. Biol.* **15**, 65–70 (2008).
6. R. Figueira, D. W. Holden, Functions of the Salmonella pathogenicity island 2 (SPI-2) type III secretion system effectors. *Microbiology (Reading)* **158**, 1147–1161 (2012).
7. M. M. Turco, M. C. Sousa, The structure and specificity of the type III secretion system effector NleC suggest a DNA mimicry mechanism of substrate recognition. *Biochemistry* **53**, 5131–5139 (2014).
8. J. S. Pearson, P. Riedmaier, O. Marchès, G. Frankel, E. L. Hartland, A type III effector protease NleC from enteropathogenic Escherichia coli targets NF-κB for degradation. *Mol. Microbiol.* **80**, 219–230 (2011).
9. A. Friebel *et al*., SopE and SopE2 from Salmonella typhimurium activate different sets of RhoGTPases of the host cell. *J. Biol. Chem.* **276**, 34035–34040 (2001).
10. C. E. Stebbins, J. E. Galán, Modulation of host signaling by a bacterial mimic: Structure of the Salmonella effector SptP bound to Rac1. *Mol. Cell* **6**, 1449–1460 (2000).
11. S. C. Birtalan, R. M. Phillips, P. Ghosh, Three-dimensional secretion signals in chaperone-effector complexes of bacterial pathogens. *Mol. Cell* **9**, 971–980 (2002).
12. Y. Luo *et al*., Structural and biochemical characterization of the type III secretion chaperones CesT and SigE. *Nat. Struct. Biol.* **8**, 1031–1036 (2001).
13. I. Bernal *et al*., Molecular organization of soluble type III secretion system sorting platform complexes. *J. Mol. Biol.* **431**, 3787–3803 (2019).
14. J. Radics, L. Königsmaier, T. C. Marlovits, Structure of a pathogenic type 3 secretion system in action. *Nat. Struct. Mol. Biol.* **21**, 82–87 (2014).
15. R. Zarivach, M. Vuckovic, W. Deng, B. B. Finlay, N. C. Strynadka, Structural analysis of a prototypical ATPase from the type III secretion system. *Nat. Struct. Mol. Biol.* **14**, 131–137 (2007).
16. A. Loquet *et al*., Atomic model of the type III secretion system needle. *Nature* **486**, 276–279 (2012).
17. R. Q. Notti, C. E. Stebbins, The structure and function of type III secretion systems. *Microbiol. Spectr.* **4**, 10.1128/microbiolspec.VMBF-0004-2015 (2016).
18. Y. Akeda, J. E. Galán, Genetic analysis of the Salmonella enterica type III secretion-associated ATPase InvC defines discrete functional domains. *J. Bacteriol.* **186**, 2402–2412 (2004).
19. S. Woestyn, A. Allaoui, P. Wattiau, G. R. Cornelis, YscN, the putative energizer of the Yersinia Yop secretion machinery. *J. Bacteriol.* **176**, 1561–1569 (1994).
20. M. F. Feldman, S. Müller, E. Wüest, G. R. Cornelis, SycE allows secretion of YopE-DHFR hybrids by the Yersinia enterocolitica type III Ysc system. *Mol. Microbiol.* **46**, 1183–1197 (2002).
21. C. L. Smith, S. J. Hultgren, Bacteria thread the needle. *Nature* **414**, 29–31, 31 (2001).
22. Y. Akeda, J. E. Galán, Chaperone release and unfolding of substrates in type III secretion. *Nature* **437**, 911–915 (2005).
23. S. M. Doyle, O. Genest, S. Wickner, Protein rescue from aggregates by powerful molecular chaperone machines. *Nat. Rev. Mol. Cell Biol.* **14**, 617–629 (2013).
24. A. O. Olivares, H. C. Kotamarthi, B. J. Stein, R. T. Sauer, T. A. Baker, Effect of directional pulling on mechanical protein degradation by ATP-dependent proteolytic machines. *Proc. Natl. Acad. Sci. U.S.A.* **114**, E6306–E6313 (2017).
25. R. A. Maillard *et al*., ClpX(P) generates mechanical force to unfold and translocate its protein substrates. *Cell* **145**, 459–469 (2011).
26. A. Peth, J. A. Nathan, A. L. Goldberg, The ATP costs and time required to degrade ubiquitinated proteins by the 26 S proteasome. *J. Biol. Chem.* **288**, 29215–29222 (2013).
27. A. R. Nager, T. A. Baker, R. T. Sauer, Stepwise unfolding of a β barrel protein by the AAA+ ClpXP protease. *J. Mol. Biol.* **413**, 4–16 (2011).
28. C. Pozidis *et al*., Type III protein translocase: HrcN is a peripheral ATPase that is activated by oligomerization. *J. Biol. Chem.* **278**, 25816–25824 (2003).
29. D. D. Majewski *et al*., Cryo-EM structure of the homohexameric T3SS ATPase-central stalk complex reveals rotary ATPase-like asymmetry. *Nat. Commun.* **10**, 626 (2019).
30. I. Bernal *et al*., Structural analysis of ligand-bound states of the Salmonella type III secretion system ATPase InvC. *Protein Sci.* **28**, 1888–1901 (2019).
31. V. T. Lee, O. Schneewind, Yop fusions to tightly folded protein domains and their effects on Yersinia enterocolitica type III secretion. *J. Bacteriol.* **184**, 3740–3745 (2002).
32. J. A. Sorg, N. C. Miller, M. M. Marketon, O. Schneewind, Rejection of impassable substrates by Yersinia type III secretion machines. *J. Bacteriol.* **187**, 7090–7102 (2005).
33. J. E. Dawson, L. K. Nicholson, Folding kinetics and thermodynamics of Pseudomonas syringae effector protein AvrPto provide insight into translocation via the type III secretion system. *Protein Sci.* **17**, 1109–1119 (2008).
34. M. S. Z. Kellermayer, S. B. Smith, H. L. Granzier, C. Bustamante, Folding-unfolding transitions in single titin molecules characterized with laser tweezers. *Science* **276**, 1112–1116 (1997).
35. C. Cecconi, E. A. Shank, C. Bustamante, S. Marqusee, Direct observation of the three-state folding of a single protein molecule. *Science* **309**, 2057–2060 (2005).
36. M. Rief, M. Gautel, F. Oesterhelt, J. M. Fernandez, H. E. Gaub, Reversible unfolding of individual titin immunoglobulin domains by AFM. *Science* **276**, 1109–1112 (1997).
37. C. Bustamante, Y. R. Chemla, N. R. Forde, D. Izhaky, Mechanical processes in biochemistry. *Annu. Rev. Biochem.* **73**, 705–748 (2004).
38. A. F. Oberhauser, C. Badilla-Fernandez, M. Carrion-Vazquez, J. M. Fernandez, The mechanical hierarchies of fibronectin observed with single-molecule AFM. *J. Mol. Biol.* **319**, 433–447 (2002).
39. M. Rief, J. Pascual, M. Saraste, H. E. Gaub, Single molecule force spectroscopy of spectrin repeats: Low unfolding forces in helix bundles. *J. Mol. Biol.* **286**, 553–561 (1999).
40. M. Carrion-Vazquez *et al*., The mechanical stability of ubiquitin is linkage dependent. *Nat. Struct. Biol.* **10**, 738–743 (2003).
41. D. J. Brockwell *et al*., Pulling geometry defines the mechanical resistance of a β-sheet protein. *Nat. Struct. Biol.* **10**, 731–737 (2003).
42. M. L. Bang *et al*., The complete gene sequence of titin, expression of an unusual approximately 700-kDa titin isoform, and its interaction with obscurin identify a novel Z-line to I-band linking system. *Circ. Res.* **89**, 1065–1072 (2001).
43. H. Li, A. F. Oberhauser, S. B. Fowler, J. Clarke, J. M. Fernandez, Atomic force microscopy reveals the mechanical design of a modular protein. *Proc. Natl. Acad. Sci. U.S.A.* **97**, 6527–6531 (2000).
44. H. Dietz, M. Rief, Exploring the energy landscape of GFP by single-molecule mechanical experiments. *Proc. Natl. Acad. Sci. U.S.A.* **101**, 16192–16197 (2004).
45. C. L. Chyan *et al*., Reversible mechanical unfolding of single ubiquitin molecules. *Biophys. J.* **87**, 3995–4006 (2004).
46. S. R. Ainavarapu, L. Li, C. L. Badilla, J. M. Fernandez, Ligand binding modulates the mechanical stability of dihydrofolate reductase. *Biophys. J.* **89**, 3337–3344 (2005).
47. C. Williams, E. E. Galyov, S. Bagby, Solution structure, backbone dynamics, and interaction with Cdc42 of Salmonella guanine nucleotide exchange factor SopE2. *Biochemistry* **43**, 11998–12008 (2004).
48. S. B. Van Engelenburg, A. E. Palmer, Quantification of real-time Salmonella effector type III secretion kinetics reveals differential secretion rates for SopE2 and SptP. *Chem. Biol.* **15**, 619–628 (2008).
49. C. E. Stebbins, J. E. Galán, Maintenance of an unfolded polypeptide by a cognate chaperone in bacterial type III secretion. *Nature* **414**, 77–81 (2001).
50. J. Clarke, A. R. Fersht, Engineered disulfide bonds as probes of the folding pathway of barnase: Increasing the stability of proteins against the rate of denaturation. *Biochemistry* **32**, 4322–4329 (1993).
51. A. D. Robertson, K. P. Murphy, Protein structure and the energetics of protein stability. *Chem. Rev.* **97**, 1251–1268 (1997).
52. R. Walder *et al*., Rapid characterization of a mechanically labile alpha-helical protein enabled by efficient site-specific bioconjugation. *J. Am. Chem. Soc.* **139**, 9867–9875 (2017).
53. C. Schoeler *et al*., Mapping mechanical force propagation through biomolecular complexes. *Nano Lett.* **15**, 7370–7376 (2015).
54. M. S. Bull, R. M. A. Sullan, H. Li, T. T. Perkins, Improved single molecule force spectroscopy using micromachined cantilevers. *ACS Nano* **8**, 4984–4995 (2014).
55. D. T. Edwards, T. T. Perkins, Optimizing force spectroscopy by modifying commercial cantilevers: Improved stability, precision, and temporal resolution. *J. Struct. Biol.* **197**, 13–25 (2017).
56. J. Yin, A. J. Lin, D. E. Golan, C. T. Walsh, Site-specific protein labeling by Sfp phosphopantetheinyl transferase. *Nat. Protoc.* **1**, 280–285 (2006).
57. M. Schlierf, F. Berkemeier, M. Rief, Direct observation of active protein folding using lock-in force spectroscopy. *Biophys. J.* **93**, 3989–3998 (2007).
58. M. D. Wang, H. Yin, R. Landick, J. Gelles, S. M. Block, Stretching DNA with optical tweezers. *Biophys. J.* **72**, 1335–1346 (1997).
59. F. Oesterhelt *et al*., Unfolding pathways of individual bacteriorhodopsins. *Science* **288**, 143–146 (2000).
60. T. Hoffmann, K. M. Tych, M. L. Hughes, D. J. Brockwell, L. Dougan, Towards design principles for determining the mechanical stability of proteins. *Phys. Chem. Chem. Phys.* **15**, 15767–15780 (2013).
61. M. L. Hughes, L. Dougan, The physics of pulling polyproteins: A review of single molecule force spectroscopy using the AFM to study protein unfolding. *Rep. Prog. Phys.* **79**, 076601 (2016).

Downloaded at CU Libraries on March 15, 2021

62. E. Evans, K. Ritchie, Dynamic strength of molecular adhesion bonds. *Biophys. J.* **72**, 1541–1555 (1997).
63. S. H. Lee, J. E. Galán, Salmonella type III secretion-associated chaperones confer secretion-pathway specificity. *Mol. Microbiol.* **51**, 483–495 (2004).
64. M. Lilic, M. Vujanac, C. E. Stebbins, A common structural motif in the binding of virulence factors to bacterial secretion chaperones. *Mol. Cell* **21**, 653–664 (2006).
65. F. D. Schubot *et al*., Three-dimensional structure of a macromolecular assembly that regulates type III secretion in Yersinia pestis. *J. Mol. Biol.* **346**, 1147–1161 (2005).
66. J. E. Dawson *et al*., Elucidation of a pH-folding switch in the Pseudomonas syringae effector protein AvrPto. *Proc. Natl. Acad. Sci. U.S.A.* **106**, 8543–8548 (2009).
67. Z. Y. Zhang *et al*., Expression, purification, and physicochemical characterization of a recombinant Yersinia protein tyrosine phosphatase. *J. Biol. Chem.* **267**, 23759–23766 (1992).
68. B. T. Andrews, A. R. Schoenfish, M. Roy, G. Waldo, P. A. Jennings, The rough energy landscape of superfolder GFP is linked to the chromophore. *J. Mol. Biol.* **373**, 476–490 (2007).
69. V. V. Loladze, B. Ibarra-Molero, J. M. Sanchez-Ruiz, G. I. Makhatadze, Engineering a thermostable protein via optimization of charge-charge interactions on the protein surface. *Biochemistry* **38**, 16419–16423 (1999).
70. S. K. Chunduru *et al*., Methotrexate-resistant variants of human dihydrofolate reductase. Effects of Phe31 substitutions. *J. Biol. Chem.* **269**, 9547–9555 (1994).
71. Z. Ganim, M. Rief, Mechanically switching single-molecule fluorescence of GFP by unfolding and refolding. *Proc. Natl. Acad. Sci. U.S.A.* **114**, 11052–11056 (2017).
72. M. Schlierf, H. Li, J. M. Fernandez, The unfolding kinetics of ubiquitin captured with single-molecule force-clamp techniques. *Proc. Natl. Acad. Sci. U.S.A.* **101**, 7299–7304 (2004).
73. G. I. Bell, Models for the specific adhesion of cells to cells. *Science* **200**, 618–627 (1978).
74. A. Snoberger, R. T. Anderson, D. M. Smith, The proteasomal ATPases use a slow but highly processive strategy to unfold proteins. *Front. Mol. Biosci.* **4**, 18 (2017).
75. P. Ghosh, Process of protein transport by the type III secretion system. *Microbiol. Mol. Biol. Rev.* **68**, 771–795 (2004).
76. U. F. Keyser *et al*., Direct force measurements on DNA in a solid-state nanopore. *Nat. Phys.* **2**, 473–477 (2006).
77. M.-E. Aubin-Tam, A. O. Olivares, R. T. Sauer, T. A. Baker, M. J. Lang, Single-molecule protein unfolding and translocation by an ATP-fueled proteolytic machine. *Cell* **145**, 257–267 (2011).
78. Á. San Martín *et al*., Knots can impair protein degradation by ATP-dependent proteases. *Proc. Natl. Acad. Sci. U.S.A.* **114**, 9864–9869 (2017).
79. F. W. Studier, Stable expression clones and auto-induction for protein production in E. coli. *Methods Mol. Biol.* **1091**, 17–32 (2014).
80. J. K. Faulk, D. T. Edwards, M. S. Bull, T. T. Perkins, Improved force spectroscopy using focused-ion-beam-modified cantilevers. *Methods Enzymol.* **582**, 321–351 (2017).
81. J. E. Sader, J. W. M. Chon, P. Mulvaney, Calibration of rectangular atomic force microscope cantilevers. *Rev. Sci. Instrum.* **70**, 3967–3969 (1999).
82. J. P. Junker, F. Ziegler, M. Rief, Ligand-dependent equilibrium fluctuations of single calmodulin molecules. *Science* **323**, 633–637 (2009).
83. L. Masino, S. R. Martin, P. M. Bayley, Ligand binding and thermodynamic stability of a multidomain protein, calmodulin. *Protein Sci.* **9**, 1519–1529 (2000).
84. P. Zheng, H. Li, Direct measurements of the mechanical stability of zinc-thiolate bonds in rubredoxin by single-molecule atomic force microscopy. *Biophys. J.* **101**, 1467–1473 (2011).
85. M. Carrion-Vazquez *et al*., Mechanical and chemical unfolding of a single protein: A comparison. *Proc. Natl. Acad. Sci. U.S.A.* **96**, 3694–3699 (1999).
86. A. F. Oberhauser, P. E. Marszalek, H. P. Erickson, J. M. Fernandez, The molecular elasticity of the extracellular matrix protein tenascin. *Nature* **393**, 181–185 (1998).
87. J. Clarke, S. J. Hamill, C. M. Johnson, Folding and stability of a fibronectin type III domain of human tenascin. *J. Mol. Biol.* **270**, 771–778 (1997).
88. H. Li, J. M. Fernandez, Mechanical design of the first proximal Ig domain of human cardiac titin revealed by single molecule force spectroscopy. *J. Mol. Biol.* **334**, 75–86 (2003).
89. K. L. Fuson, L. Ma, R. B. Sutton, A. F. Oberhauser, The c2 domains of human synaptotagmin 1 have distinct mechanical properties. *Biophys. J.* **96**, 1083–1090 (2009).
90. M. E. Fealey *et al*., Negative coupling as a mechanism for signal propagation between C2 domains of synaptotagmin I. *PLoS One* **7**, e46748 (2012).
91. K. W. Plaxco, C. Spitzfaden, I. D. Campbell, C. M. Dobson, A comparison of the folding kinetics and thermodynamics of two homologous fibronectin type III modules. *J. Mol. Biol.* **270**, 763–770 (1997).
92. D. Wassenberg, C. Welker, R. Jaenicke, Thermodynamics of the unfolding of the cold-shock protein from Thermotoga maritima. *J. Mol. Biol.* **289**, 187–193 (1999).
93. I. Schwaiger, A. Kardinal, M. Schleicher, A. A. Noegel, M. Rief, A mechanical unfolding intermediate in an actin-crosslinking protein. *Nat. Struct. Mol. Biol.* **11**, 81–85 (2004).
94. M. Schlierf, M. Rief, Single-molecule unfolding force distributions reveal a funnel-shaped energy landscape. *Biophys. J.* **90**, L33–L35 (2006).
95. Y. Cao, M. M. Balamurali, D. Sharma, H. Li, A functional single-molecule binding assay via force spectroscopy. *Proc. Natl. Acad. Sci. U.S.A.* **104**, 15677–15681 (2007).
96. P. Alexander, S. Fahnestock, T. Lee, J. Orban, P. Bryan, Thermodynamic analysis of the folding of the streptococcal protein G IgG-binding domains B1 and B2: Why small proteins tend to have high denaturation temperatures. *Biochemistry* **31**, 3597–3603 (1992).
97. D. Sharma *et al*., Single-molecule force spectroscopy reveals a mechanically stable protein fold and the rational tuning of its mechanical stability. *Proc. Natl. Acad. Sci. U.S.A.* **104**, 9278–9283 (2007).
98. B. Kuhlman *et al*., Design of a novel globular protein fold with atomic-level accuracy. *Science* **302**, 1364–1368 (2003).
99. D. J. Brockwell *et al*., Mechanically unfolding the small, topologically simple protein L. *Biophys. J.* **89**, 506–519 (2005).
100. M. L. Scalley *et al*., Kinetics of folding of the IgG binding domain of peptostreptococcal protein L. *Biochemistry* **36**, 3373–3382 (1997).
101. C. He, G. Z. Genchev, H. Lu, H. Li, Mechanically untying a protein slipknot: Multiple pathways revealed by force spectroscopy and steered molecular dynamics simulations. *J. Am. Chem. Soc.* **134**, 10428–10435 (2012).
102. R. B. Best, B. Li, A. Steward, V. Daggett, J. Clarke, Can non-mechanical proteins withstand force? Stretching barnase by atomic force microscopy and molecular dynamics simulation. *Biophys. J.* **81**, 2344–2356 (2001).
103. C. M. Johnson, A. R. Fersht, Protein stability as a function of denaturant concentration: The thermal stability of barnase in the presence of urea. *Biochemistry* **34**, 6795–6804 (1995).
104. G. Arad-Haase *et al*., Mechanical unfolding of acylphosphatase studied by single-molecule force spectroscopy and MD simulations. *Biophys. J.* **99**, 238–247 (2010).
105. N. Taddei *et al*., Equilibrium unfolding studies of horse muscle acylphosphatase. *Eur. J. Biochem.* **225**, 811–817 (1994).
106. X. Gao *et al*., Single-molecule experiments reveal the flexibility of a Per-ARNT-Sim domain and the kinetic partitioning in the unfolding pathway under force. *Biophys. J.* **102**, 2149–2157 (2012).
107. M. R. Evans, P. B. Card, K. H. Gardner, ARNT PAS-B has a fragile native state structure with an alternative β-sheet register nearby in sequence space. *Proc. Natl. Acad. Sci. U.S.A.* **106**, 2617–2622 (2009).
108. J. M. Dabora, S. Marqusee, Equilibrium unfolding of Escherichia coli ribonuclease H: Characterization of a partially folded state. *Protein Sci.* **3**, 1401–1408 (1994).
109. L. A. Horvath, J. M. Sturtevant, J. H. Prestegard, Kinetics and thermodynamics of thermal denaturation in acyl carrier protein. *Protein Sci.* **3**, 103–108 (1994).
110. K. S. Thompson, C. R. Vinson, E. Freire, Thermodynamic characterization of the structural stability of the coiled-coil region of the bZIP transcription factor GCN4. *Biochemistry* **32**, 5491–5496 (1993).
111. Y. Hagihara, M. Oobatake, Y. Goto, Thermal unfolding of tetrameric melittin: Comparison with the molten globule state of cytochrome c. *Protein Sci.* **3**, 1418–1429 (1994).
112. H. J. Hinz, M. Cossmann, K. Beyreuther, Lac Repressor headpiece constitutes a reversibly unfolding domain. *FEBS Lett.* **129**, 246–248 (1981).
113. L. Kelly, L. A. Holladay, A comparative study of the unfolding thermodynamics of vertebrate metmyoglobins. *Biochemistry* **29**, 5062–5069 (1990).
114. S. J. Bae, W. Y. Chou, K. Matthews, J. M. Sturtevant, Tryptophan repressor of Escherichia coli shows unusual thermal stability. *Proc. Natl. Acad. Sci. U.S.A.* **85**, 6731–6732 (1988).
115. V. V. Novokhatny, S. A. Kudinov, P. L. Privalov, Domains in human plasminogen. *J. Mol. Biol.* **179**, 215–232 (1984).
116. M. Renner, H. J. Hinz, M. Scharf, J. W. Engels, Thermodynamics of unfolding of the alpha-amylase inhibitor tendamistat. Correlations between accessible surface area and heat capacity. *J. Mol. Biol.* **223**, 769–779 (1992).

Downloaded at CU Libraries on March 15, 2021